J6.1 THE DEVELOPMENT OF THE FIRST-ORDER TIME EXTRAPOLATION TO THE OBSERVATION (FOTO) METHOD AND ITS APPLICATION IN THE NCEP GLOBAL DATA ASSIMILATION SYSTEM

Miodrag Rančić,* John C. Derber, Dave Parrish, Russ Treadon, and Daryl T. Kleist
EMC/NCEP Camp Springs, Maryland

1. INTRODUCTION

This paper presents the FOTO method and its implementation in the GSI (Wu et al. 2002). The objective of FOTO (First-Order Time extrapolation to the Observation) is to represent observations at their appropriate times within the analysis interval of the GSI (Gridpoint Statistical Interpolation) without substantially increasing the cost. The FOTO method applies a low order (first order in this case) approximation to describe the time evolution of the analysis variables over the analysis time. This idea has been around the NCEP for some time, and the reported development capitalizes on the previous work of many collaborators.

In section 2 we provide a brief theoretical background for the development of FOTO, pointing at differences between FOTO and 4DVAR. We also briefly describe the method for calculation of time tendencies, including a simple parameterization of the PBL. A review of the preliminary results, including the effects of FOTO on fitting various types of observations in the GSI global analysis, are presented in section 3. Concluding section 4 contains a summary and a discussion of the secondary effects of FOTO on the GSI analysis.

2. THEORETICAL BACKGROUND

2.1. 3DVAR

The three-dimensional variational data assimilation (3DVAR) that has been taken as a framework for the development of GSI, estimates initial state of the atmosphere as the minimum of the cost function:

$$\begin{aligned} J(\mathbf{x}) &= \tfrac{1}{2}\left(\mathbf{z}-h(\mathbf{x})\right)^T \mathbf{R}^{-1}\left(\mathbf{z}-h(\mathbf{x})\right) \\ &+ \tfrac{1}{2}\left(\mathbf{x}-\mathbf{x_b}\right)^T \mathbf{B}^{-1}\left(\mathbf{x}-\mathbf{x_b}\right) \end{aligned} \tag{1}$$

Here, vector $\mathbf{x}$ represents the analyzed fields, $\mathbf{z}$ observations, $h(\mathbf{x})$ is the 'forward operator' expressing the observed variables in terms of the analyzed fields, and $\mathbf{x_b}$ is the background field. Matrices $\mathbf{R}$ and $\mathbf{B}$ represent error covariances, the first one of the measurements and of the forward operator, and the second of the background field.

In the traditional implementation of 3DVAR there is no place for inclusion of the temporal distribution of observations, and the difference between the observations and the background is assumed constant over the analysis time interval. With an explosive increase of the number of non-conventional datasets, such as satellite radiances (e.g., Derber and Wu 1998; Okamoto and Derber 2006; Le Marshall et al. 2001) or Global Positioning System (GPS) radio occultations (e.g., Cucurull et al. 2007), there is a desire to improve the realism of the analysis by recognizing temporal distribution of data available for assimilation, even within a 3DVAR data assimilation approach. Figure 1. shows as an example the time distribution of the surface pressure data used in the GSI.

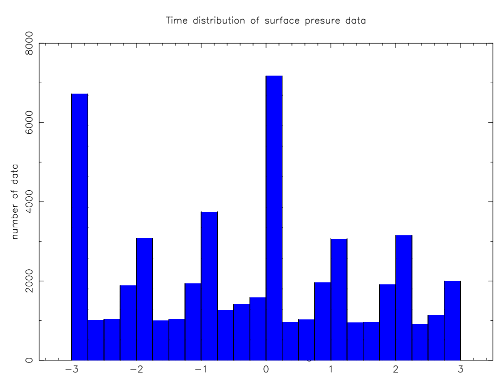

Figure 1: Distribution of the surface pressure data within the analysis time window. The data are sampled in 15 min intervals.

*Corresponding author address: Miodrag Rančić, SAIC/NCEP/EMC, 5200 Auth Rd, Rm 705, Camp Springs, MD 20746, miodrag.rancic@noaa.edu

2.2. 4DVAR

The standard way for taking into account the distribution of data in time within a data assimilation system is application of the four-dimensional variational data assimilation (4DVAR) (e.g., Rabier et al. 2000; Zou et al. 2001; Zupanski et al. 2000; Gauthier et al. 2007; Rawlins et al. 2007). 4DVAR is much more expensive than 3DVAR, and in the major centers it is generally applied at lower resolutions than the forecasting models.

2.3. FOTO

The essence of the FOTO method is to modify the first term in the formulation of the objective function, J_o, by taking into account position of the observation in time:

$$J_o(\mathbf{x}) = \frac{1}{2} \quad \begin{array}{l} \left(\mathbf{z} - h(\mathbf{x} + \left(\frac{\partial \mathbf{x}}{\partial t}\right)_F \Delta t)\right)^T \mathbf{R^{-1}} \\ \left(\mathbf{z} - h(\mathbf{x} + \left(\frac{\partial \mathbf{x}}{\partial t}\right)_F \Delta t)\right) \end{array} \tag{2}$$

Here, Δt is the time increment of the observation $\mathbf{z}$ relative to the analysis time, and $\left(\frac{\partial \mathbf{x}}{\partial t}\right)_F$ are filtered time tendencies of the analysis at the points surrounding this observation. Consequently, while stepping through the preconditioned conjugate gradient algorithm, in the calculations of the gradient of the objective function, search direction and the step size, the effect of the filtered time tendencies is consistently taken into account.

The inclusion of the FOTO in GSI did not significantly increase the computational cost. Table 1 shows the wall clock times for GSI applied to global analysis. FOTO increases the computational costs of GSI about 8-9%, a half of which is attributed to the PBL parameterization. Thus, FOTO is including the time dimension into analysis while allowing GSI to run at the same resolution as the forecasting models.

	no foto	no pbl	with pbl
time (s)	1824.4	1907.3	1992.2
%		4.26	8.42

Table 1: Average wall clock times for GSI analysis with and without FOTO.

2.4. Time tendencies

The time tendencies are designed by a spatial discretization of the governing equations for a dry, adiabatic atmosphere, and were originally included in GSI in order to define the dynamical constraints, attempting to improve the balance of the GSI analysis. High order compact differencing is applied in the horizontal directions. The conservative vertical finite-differencing scheme, combined with a generalized vertical coordinate (Juang 2005), the same as in the latest version of the GFS (Global Forecasting System), is applied in the vertical direction. In the last update of GSI, the incremental balance of the analysis produced by GSI has been achieved by the inclusion of a tangent linear normal mode constraint (Kleist et al. 2008), and the tendencies are filtered by the projection onto the slow modes.

2.5. Inclusion of PBL

A simplistic parameterization of the planetary boundary layer (PBL) is added to the definition of time tendencies with inclusion of FOTO. It is based on the Janjić (1990) implementation of Mellor and Yamada (1974) 2.0 closure scheme. This PBL parameterization is sufficiently simple to allow relatively quick calculation of a tangent linear version and its adjoint, but still complex enough to describe elements of turbulent mixing as a function of both thermal and dynamical conditions of the atmosphere. During development of the tangent linear version of the parameterization, additional simplifications were made. The most notable one was the 'assumption of the K-theory', which consisted of neglecting the vertical derivatives of turbulent coefficients (Dusanka Zupanski, personal communications). This approximation reduced the nonlinearity of the parameterization, and resulted in more realistic account of the PBL within the GSI analysis.

3. RESULTS

3.1. Single case

A series of individual analyses were prepared. All of them indicate approximately similar impacts of FOTO. Instead of calculating average diagnostics of all analyzed cases, we present here just the analysis from 4/10/2007, as a typical case. Furthermore, We focus only at a *cpen* diagnostic, defined as the penalty term normalized by the number of observations.

Tables 2, 3 and 4 give respectively the normalized penalty for pressure, ozone and radiances. Figures 2 and 3 present the *cpen* for the wind and the temperature data.

The analysis with FOTO improves matching of all presented types of data, even up to 30% and more in some cases (for example, for the ozone data). The inclusion of PBL brings additional sense of the reality in the analysis, especially in the lower atmosphere as may be expected. However, the effect on the moisture, though consistently positive, is very small (about 2-3%), presumably because a large portion of the moisture data is coming from the radiosonde measurements.

	no foto	no pbl	with pbl
cpen	0.1225	0.1186	0.1174
%		-3.18	-4.16

Table 2: Diagnostics *cpen* for the surface pressure data.

satell./ instr.	no foto	with pbl	%
n16 / sbuv2	0.86343	0.62250	-27.9
n17 / sbuv2	0.79763	0.49344	-38.13

Table 3: Diagnostics *cpen* for the ozone data.

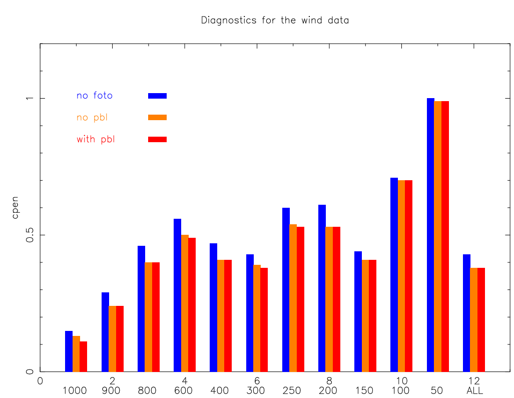

Figure 2: Normalized penalty (*cpen*) for the wind data in the GSI analysis after inclusion of FOTO.

3.2. Parallel run

A series of cycling experiments with FOTO has been run (and some are still running) at NCEP, indicating that FOTO has generally a neutral or a positive impact on the GSI analysis and the subsequent forecasts, especially in the Southern Hemisphere. We assume that this is a consequence of an improved representation of the satellite data that prevail in that region. Final evaluation of the quality of the analysis/forecast is still underway.

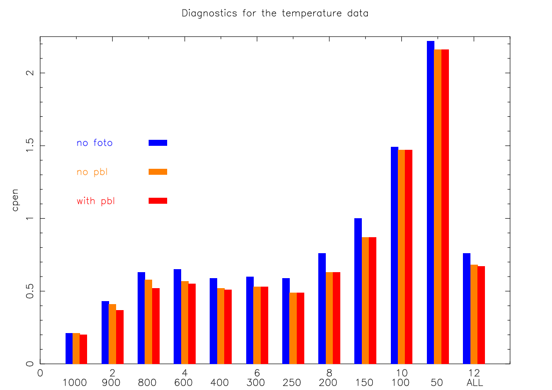

Figure 3: Normalized penalty (*cpen*) for the temperature data in the GSI analysis after inclusion of FOTO.

4. CONCLUSION AND DISCUSSION

FOTO is a relatively efficient technique for taking into account temporal distribution of the observations within a 3DVAR data assimilation system. It was successfully implemented in the GSI, and the preliminary tests generally demonstrate a positive impact of the FOTO on the produced analyses.

We also noticed that FOTO tends to reduce somewhat the convergence rate of the preconditioned conjugate gradient algorithm applied in GSI. Figure 4 shows a measure of the convergence (*gnorm*) in the single test case presented above with and without FOTO.

satell./ instr.	no foto	with pbl	%
n17 / hirs3	0.30188	0.27604	-8.56
aqua / airs	0.19756	0.19178	-2.93
n15 / amsua	0.14379	0.13199	-8.21
n16 / amsua	0.04683	0.04546	-2.91
n18 / amsua	0.13663	0.12788	-6.40
aqua / amsua	0.13868	0.13133	-5.30
n15 / amsub	0.12174	0.10681	-12.26
n16 / amsub	0.1183	0.10982	-7.17
n17 / amsub	0.1471	0.12154	-17.38
n18 / mhs	0.11271	0.08874	-21.27
g12 / sndrd1	0.17202	0.15805	-8.12
g12 / sndrd2	0.15474	0.14504	-6.27
g12 / sndrd3	0.14332	0.13249	-7.56
g12 / sndrd4	0.13801	0.12481	-9.56
g11 / sndrd1	0.15064	0.14196	-6.76
g11 / sndrd2	0.12282	0.11969	-2.55
g11 / sndrd3	0.11344	0.10563	-6.88
g11 / sndrd4	0.17022	0.16313	-4.11

Table 4: Diagnostics *cpen* for the radiances.

In order to improve the convergence, we experimented with various numbers for the outer and the inner iterations within GSI. Using three instead of two outer loops, with an increasing number of inner iterations in each of them, improved the convergence rate. In the current operational version, GSI has two standard outer loops, but with more inner iterations (150 instead 100) in the second outer loop, which may be sufficient to offset the FOTO's degradation of the convergence.

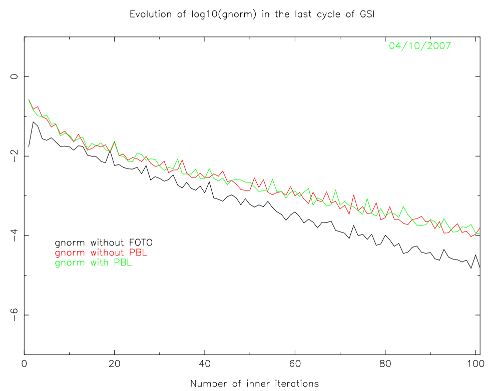

Figure 4: Evolution of a measure of convergence within the last outer iteration in the test with and without FOTO.

The tangent linear normal mode constraint was introduced in GSI in May of 2007, replacing a former balance constraint, and with it, the performance of the FOTO generally improved.

References

Cucurull, L., J. Derber, R. Treadon, and R. Purser, 2007: Assimilation of global positioning system radio occultation observations into NCEP's global data assimilation system. *Mon. Wea. Rev.*, **135**, 3174–3193.

Derber, J. C. and W.-S. Wu, 1998: The use of TOVS cloud-cleared radiances in the NCEP SSI analysis system. *Mon. Wea. Rev.*, **126**, 2287–2288.

Gauthier, P., M. Tanguay, S. Laroche, S. Pellerin, and J. Morneau, 2007: Extension of 3DVAR to 4DVAR: Implementation of 4DVAR at the Meteorological Service of Canada. *Mon. Wea. Rev.*, **135**, 2339–2354.

Janjić, Z., 1990: The step-mountain coordinate physical package. *Mon. Wea. Rev.*, **118**, 1429–1443.

Junag, H.–M. H., 2005: Discrete generalized hybrid vertical coordinates by a mass, energy and angular momentum conserving vertical finite-difference scheme. *NCEP Office Note 445*, 35pp.

Le Marshall, J. and co–authors, 2001: Improving global analysis and forecasting with AIRS. *Bull. Amer. Meteor. Soc.*, **87**, 891–894.

Kleist D.T., J.C. Derber, R. Treadon, D. Parrish, R. Errico, and R. Yang, 2008: Improving incremental balance in the GSI 3DVAR analysis system. *Mon. Wea. Rev.*, in preparation.

Mellor, G. L. and T. Yamada, 1974: A hierarchy of turbulence closure models for planetary boundary layers. *J. Atmos. Sci.*, **31**, 1791–1806.

Okamoto, K. and J. C. Derber, 2006: Assimilation of SSM/I radiances in the NCEP global data assimilation system. *Mon. Wea. Rev.*, **134**, 2612–2631.

Rabier, F., H. Järvinen, E. Klinker, J.-F. Mahfouf, and A. Simons, 2000: The ECMWF operational implementation of four dimensional variational assimilation. Part 1: Experimental results with simplified physics. *Quart. J. Roy. Meteor. Soc.*, **126**, 1143–1170.

Rawlins, F., S. Ballard, K. Bovis, A. Clayton, D. Li, G. Inverarity, A. A.C. Lorenc, and T. J. Payne, 2007: The Met Office global four-dimensional variational data assimilation scheme. *Quart. J. Roy. Meteor. Soc.*, **133**, 347–362.

Wu, W.-S., R. J. Purser, and D. Parish, 2002: Three-dimensional variational analysis with spatially inhomogeneous covariances. *Mon. Wea. Rev.*, **130**, 2905–2916.

Zou, X., H. Liu, J. Derber, J. Sela, R. Treadon, I. Navon, and B. Wang, 2001: Four-dimensional variational data assimilation with a diabatic version of the NCEP global spectral model: System development and preliminary results. *Quart. J. Roy. Meteor. Soc.*, **123**, 1095–1122.

Zupanski, M., D. Zupanski, D. Parrish, E. Rogers, and G. DiMego, 2000: Four-dimensional variational data assimilation for the Blizzard of 2000. *Mon. Wea. Rev.*, **130**, 1967–1988.